Input-Output Analysis and Control Design of Spatially Developing Shear Flows

S. Bagheri [*], E. Åkervik[†], L. Brandt[‡] and D.S. Henningson[§]

Linné Flow Centre, Department of Mechanics,

Royal Institute of Technology, SE-100 44, Stockholm, Sweden

A framework for the input-output analysis, model reduction and control design of spatially developing shear flows is presented using the Blasius boundary-layer flow as an example. An input-output formulation of the governing equations yields a flexible formulation for treating stability problems and for developing control strategies that optimize given objectives. Model reduction plays an important role in this process since the dynamical systems that describe most flows are discretized partial differential equations with a very large number of degrees of freedom. Moreover, as system theoretical tools, such as controllability, observability and balancing has become computationally tractable for large-scale systems, a systematic approach to model reduction is presented.

I.   Introduction

Control of wall-bounded transitional and turbulent flows has been the subject of several research efforts owing to the high potential benefits. In these fluid-mechanics systems, due to the large flow sensitivity, dramatic effects on global flow parameters may be achieved by minute local perturbations using devices sensing and acting on only small parts of the flow with a small amount of energy. Such control devices can be used to obtain reduction of the skin-friction drag, for example, implying relevant savings of the operational cost of commercial aircrafts and cargo ships.

In this paper we present a framework for the input-output analysis, model reduction and control design for complex flows. As a prototype of spatially developing shear flows the Blasius boundary-layer flow is considered. The work is motivated by the need to provide efficient numerical tools to analyze complex flows and design efficient control strategies. Powerful tools from linear systems and control theory could not be used for fluid flows due to the complexity of the Navier–Stokes equations. However, the availability of increasingly powerful computer resources and recent advances of matrix-free methods now enables the application of analytical techniques that do not rely on physical insight into the specific flow configuration and can in principle be applied to any geometry. The methods presented here all rely on the availability of a numerical code for the solution of the Navier-Stokes equations and of the corresponding adjoint problem.

It is now well understood that the wall-bounded flows are very sensitive to specific perturbations.[1] In particular, boundary layer flows support convective instabilities and behave as noise amplifiers.[2] Convectively unstable shear flows are in fact stable from a global point of view:[2,3] wave packets can be generated locally, grow in amplitude while traveling downstream and finally decay or leave the observation window. This behavior can be captured by a non-modal analysis, see e.g. Ref. 4. It is therefore meaningful to analyze the flow response from an input-output perspective. This provides knowledge on the spatial structure of the initial conditions and forcing yielding largest possible energy growth over a finite time interval. This optimization problem can be solved efficiently for more complex flows by solving the direct and adjoint Navier-Stokes equation for the linear evolution of perturbation about a steady state, as shown here (see also Ref. 5).

---

[*]Ph.D. Candidate, Mechanics, Student Member.
[†]Ph.D. Candidate, Mechanics, Student Member.
[‡]Assistant Professor, Mechanics.
[§]Professor, Mechanics, Member AIAA.

American Institute of Aeronautics and Astronautics

In the context of hydrodynamic stability, the input/output approach usually considers the flow subject to initial condition or forcing whose spatial structure is the object of the optimization mentioned above. However, to perform model reduction realistic inputs and outputs have to be considered in order to represent the system behavior in its actual configuration. Model reduction becomes indeed essential to apply modern control theory in fluid flow systems. The aim is to build a model of low dimension that captures the input-output behavior of the system and use this model for optimal feedback control design. With the help of the adjoint Navier–Stokes equations two fundamental dynamical structures can be identified; the flow structures most easily influenced by the actuators considered and the flow structures to which the outputs are most sensitive. These so-called controllable and observable structures determine the input-output behavior completely for linear systems. It is well-known that these two set of modes can be balanced,[6] and represented by one set of non-orthogonal modes, called the balanced modes. These are used as a projection basis for model reduction. The approximated method employed to compute the balanced modes is the snapshot-based balanced truncation.[7,8] This method has been recently applied to the channel flow [9] and the flow around a pitching airfoil.[10]

Recently, several groups have suggested and pursued the combination of computational fluid dynamics and control theory, thus going past early attempts of flow control based on physical intuition or on a trial-and-error basis (see the review in Ref. 11). In early work from our group,[12,13] a linear model-based feedback control approach, that minimizes an objective function which measures the perturbation energy, is formulated where the Orr-Sommerfeld and Squire equations model the flow dynamics. The latter equations describe the linear evolution of perturbations evolving in a parallel base flow. The control problem is combined with a state estimator: The so called Kalman and extended Kalman filter have been implemented in order to reconstruct the flow in an optimal manner by only considering continuous wall measurements. These studies have also shown the importance of physically relevant stochastic models for the estimation problem,[14,15] where stochastic noise needs to describe accurately enough the unmodeled dynamics, like uncertainties and nonlinearities. Based on these models the estimator is shown to work for both infinitesimal as well as finite amplitude perturbations in direct numerical simulations of transitional flows.[16,17] These studies however assumed a parallel base flow and distributed sensing and actuation at the wall.

Two aspects of the control problem have been identified as crucial in order to apply feedback control in more complex flows moving towards a possible implementation in wind-tunnel tests. They are i) model reduction to significantly decrease the cost of both constructing the controller and running it online, thus allow the fast computation of the control signal directly from the sensor output; ii) the need to naturally consider localized sensors and actuators. These are addressed in this work by using global modes, balanced modes in particular, to build an efficient low-order model to be used to compute the control signal.

The present works applies and extends tools for feedback control and model reduction previously applied to the complex Ginzburg-Landau equation, a model problem for non-normal spatial inhomogeneous flows which allows us to consider globally unstable flows such as the cavity flow and the flow around a cylinder as well as convectively unstable flows such as jets and boundary layers.[18]

II.   Input-Output Formulation

We consider the two-dimensional incompressible flow over a flat plate with constant free-stream velocity U_∞ as shown in Figure 1. Starting from the leading edge a viscous boundary layer evolves downstream. The evolution of the streamwise velocity u, the wall-normal velocity v and the pressure p in time and space is governed by the incompressible non-linear Navier–Stokes equation.[19] Our analysis deals with the evolution of linear perturbations on the laminar boundary layer solution and is limited to the computational domain shown by the gray area in the figure: The inflow boundary is set to the downstream position corresponding to a Reynolds number $Re_{\delta_0^*} = U_\infty \delta_0^* / \nu = 1000$, where δ_0^* is the local displacement thickness of the boundary layer and ν is the kinematic viscosity. Throughout the paper all variables are non-dimensionalized by U_∞ and δ_0^*. The length and height of the domain are $L_x = 1000$ and $L_y = 30$ in the streamwise direction x and wall-normal direction y, respectively. The equations are solved by a pseudo-spectral Direct Numerical Simulation (DNS) code described in Ref. 20, where the spatial operators are approximated by Fourier expansion in the streamwise direction with $N_x = 768$ equally distributed points and Chebyshev expansion in the wall-normal direction on $N_y = 101$ collocation points. A fringe region enforces periodicity in the streamwise direction.[20] By marching the DNS in time we obtain a steady state, about which a linearization is performed. The linearized Navier–Stokes equations will in this paper be subject to input-output analysis, model reduction

American Institute of Aeronautics and Astronautics
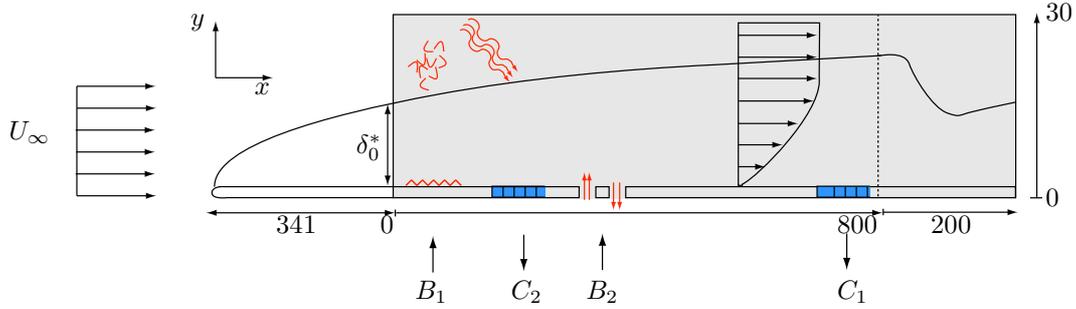
Figure 1. The input/output configuration used for the control of perturbations in a two-dimensional flat-plate geometry. The computational domain $\Omega = (0, L_x) \times (0, L_y)$, shown by the gray region, extends from $x = 0$ to $x = 1000$ with the fringe region starting at $x = 800$. The first input B_1, located at $(x_w, y_w) = (35, 1)$, models the initial receptivity phase, where disturbances are induced by free-stream turbulence, acoustic waves or wall roughness. The actuator, B_2, provides a mechanism to manipulate the flow, in this case by a localized volume forcing, and is centered at $(x_u, y_u) = (400, 1)$. Two sensors, C_1 and C_2, are located at $(x_v, y_v) = (300, 1)$ and $(x_z, y_z) = (750, 1)$ respectively. The upstream measurements are used to estimate the incoming perturbations, while the downstream sensor quantifies the effect of the control. Note that in this work all the inputs and outputs are Gaussian functions.

by approximate balanced truncation and control in the $\mathcal{H}_2$ framework. To this end we introduce the inputs $B = [B_1, B_2]$ and the ouputs $C = [C_1, C_2]$ as seen schematically in Figure 1. The first input B_1 models typical upstream disturbances entering the boundary layer through some receptivity mechanism such as freestream turbulence or acoustic waves interacting with roughness. The actuator B_2 provides a mechanism to manipulate the flow, in this case by a localized volume forcing. The upstream measurement C_1 is used to estimate the incoming perturbations, while the downstream sensor C_2 quantifies the effect of the control. Note that in this work all the inputs and outputs are Gaussian functions on both velocity components given by the expression

$$\begin{bmatrix} \sigma_x \gamma_y \\ -\sigma_y \gamma_x \end{bmatrix} \exp(-\gamma_x^2 - \gamma_y^2), \qquad \gamma_x = \frac{x - x_0}{\sigma_x}, \qquad \gamma_y = \frac{y - y_0}{\sigma_y}, \tag{1}$$

with (σ_x, σ_y) determening the width and height of the function and (x_0, y_0) determening its position.

Once discretized and projected onto a divergence free subspace the linearized Navier–Stokes equations for the disturbances $q = [u, v]^T$ of dimension $n \times 1$, with $n = 2N_x N_y$, can be written as

$$\frac{\mathrm{d}q}{\mathrm{d}t} = Aq + Bf, \tag{2}$$

$$y = Cq, \tag{3}$$

$$q(0) = q_0. \tag{4}$$

Here we have introduced the input operator B of dimension $n \times 2$ and the output operator C of dimension $2 \times n$. The formal solution to this system of equations is

$$y(t) = Ce^{At}q_0 + \int_0^t Ce^{A(t-\tau)}Bf(\tau)\,\mathrm{d}\tau\,. \tag{5}$$

The first part of the above relation describes the output generated by the evolution of the initial condition q_0 while the second term describes the response to the forcing B with time dependent signals f. The evaluation of the matrix exponential $\mathcal{T}(t) = e^{At}$ in (5) is the key to both stability analysis, input-output analysis and control design, all of which will be discussed in the subsequent sections. However, this operator also poses the greatest computational challenge due its dimension. The dimension, n, of the linearized operator depends on the number of non-homogeneous spatial directions of the base flow. Except for one-dimensional base flows the exponential matrix must be approximated. The simplest methods require that all elements of the matrix can be stored in memory,[21] a requirement that cannot in general be met in fluid systems. As an example, the storage of the one dimensional Orr-Sommerfeld matrix for the evolution of disturbances in parallel flows requires approximately 1MB of memory, the system matrix for the present spatially inhomogeneous flow with the numerical scheme introduced above requires approximately 200GB, while the memory usage for a full three-dimensional system would be of the order of 200TB. However, the action of $\mathcal{T}(t)$ on any flow field

American Institute of Aeronautics and Astronautics

simply represents integrating the Navier-Stokes equations in time and therefore the exponential matrix can be approximated by numerical simulation of the governing equations, also referred to as a time-stepper. In what follows the reader should equate $\mathcal{T}(t+T)q(t)$ with a DNS simulation starting with an initial condition $q(t)$ and providing $q(t+T)$ at a later time. In this so called "timestepper approach", system matrices are never stored and storage demands in memory are of the same order as a small number of flow fields.

III.   Stability Analysis

The first step in the understanding of the fluid problem at hand and in the control design is examining the hydrodynamic stability of the flow. This amounts to focusing on the initial value problem defined by the operator A in (5) with the output being the entire state. The asymptotic response of the system is governed by the eigenmodes of the evolution operator

$$\sigma_j \phi_j = \mathcal{T}(t)\phi_j. \tag{6}$$

In particular if there are eigenvalues $\sigma_j > 1$, the system is linearly globally unstable, supporting self-sustained oscillations. The above equation has the same eigenvectors as A and the eigenvalues of that system can be related to the above through $\lambda_j = \ln(\sigma_j)/t$. As now well understood the amount of information obtained from (6) is limited to the asymptotic $t \to \infty$ flow response and does not reveal the rich short time behavior. Relevant transient growth[1] of perturbations is indeed observed for almost all fluid dynamical systems and it is related to the non-normality of the operator A. Therefore, in order to examine the largest possible disturbance growth due to all possible unit norm initial conditions q_0 we will consider the amplitude of the disturbance at any time

$$||q(t)|| = (\mathcal{T}(t)q_0, \mathcal{T}(t)q_0) = (q_0, \mathcal{T}^*(t)\mathcal{T}(t)q_0). \tag{7}$$

In the expression above the adjoint evolution operator $\mathcal{T}^*(t)$ is introduced. Applying this operator corresponds to the integration of an adjoint state from time t to time 0. For a derivation of the adjoint evolution operator we refer to Ref. 22 or Ref. 23. The maximum norm of the above expression can be obtained as the largest eigenvalue of the positive definite operator $\mathcal{T}^*(t)\mathcal{T}(t)$

$$\sigma_j \phi_j = \mathcal{T}^*(t)\mathcal{T}(t)\phi_j, \tag{8}$$

with the unit norm eigenvector ϕ_j being the corresponding optimal initial condition.

The eigenvalue problems defined in (6) and (8) provide information about the modal and non-modal flow behavior. The dimension of the matrices appearing in (6) and (8) is too large to be solved by the standard QR method. Instead one has to resort to subspace methods, such as the Arnoldi or the Lanczos method,[24] that highlight the part of the spectrum that is assumed to be relevant for describing the dynamics. The essential step in both is to represent the action of the system matrix on a random vector in terms of a set of normalized Krylov vectors. Further, since it is only the action of the matrix involved that is needed, it becomes clear that one can utilize a time-stepping technique, in our case a DNS, to build the Krylov subspace.

In the two-dimensional Blasius boundary layer flow the memory requirements are still small enough to enable the storage of A in memory, so the leading eigenmodes from the matrix eigenvalue problem $\lambda_j \phi_j = A\phi_j$ can be obtained by means of the shift and invert Arnoldi procedure. Figure 2a shows the eigenvalues obtained by the shift and invert matrix method as black stars. From this figure we can identify several branches which all can be related to the spectrum of a parallel Blasius boundary layer, as found by solving the Orr-Sommerfeld equations, though modified by non-parallelism and boundary conditions.[25] The upper branch can be identified as pure Tollmien-Schlichting (TS) waves. These modes are characterized by slightly damped eigenvalues with the corresponding eigenvectors obtaining their maximum values inside the boundary layer while decaying exponentially in the free stream. Figure 2b and figure 2c show two examples of eigenvectors associated with eigenvalues marked k_1 and k_2 in Figure 2a. The streamwise wavelength of the eigenvectors increases as we go towards lower frequencies. The wall normal structures of these modes are very similar to those obtained by local temporal analysis. The timestepper method (shown as magenta circles in Figure 2a) successfully locates the slightly damped eigenvalues in perfect agreement with the ones obtained by the matrix method. It is noteworthy that all the eigenvalues are damped, indicating that we will never observe the evolution of single eigenmodes in the flow, but rather we should focus our attention on the non-modal behavior, in other words one should consider transient growth scenario. Note that it is

American Institute of Aeronautics and Astronautics
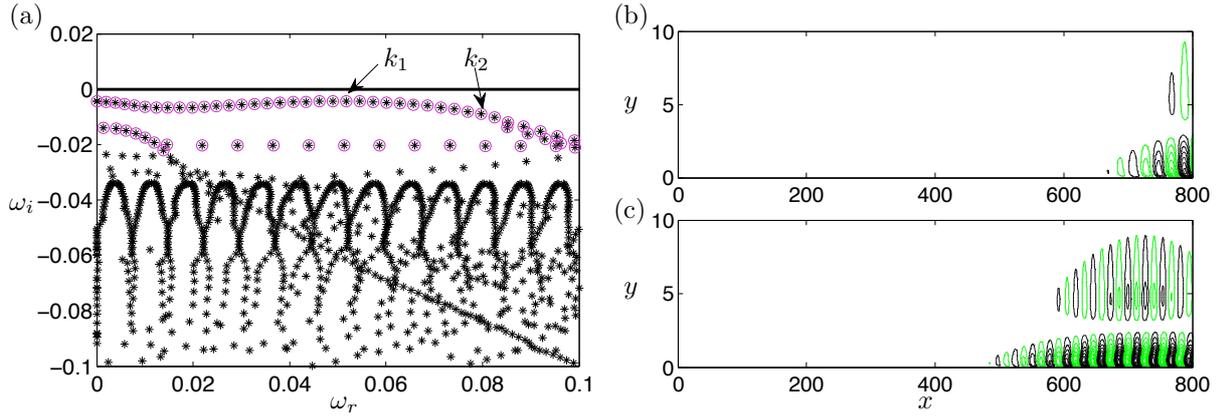
Figure 2. (a) Eigenvalues of A as computed by the shift and invert Arnoldi method (shown as black stars) and eigenvalues computed with the matrix-free method using the evolution operator $\mathcal{T}(t) = e^{At}$ (shown as magenta circles). The matrix method is capable of finding eigenvalues deeper into the damped region. The slightly damped eigenvalues, corresponding to Tollmien-Schlichting (TS) modes, and the freestream propagating modes are found by both methods. (b) Streamwise velocity component of the least stable TS eigenvectors, marked k_1 in (a). (c) Streamwise velocity component of higher frequency more damped TS mode, marked k_2 in (a).
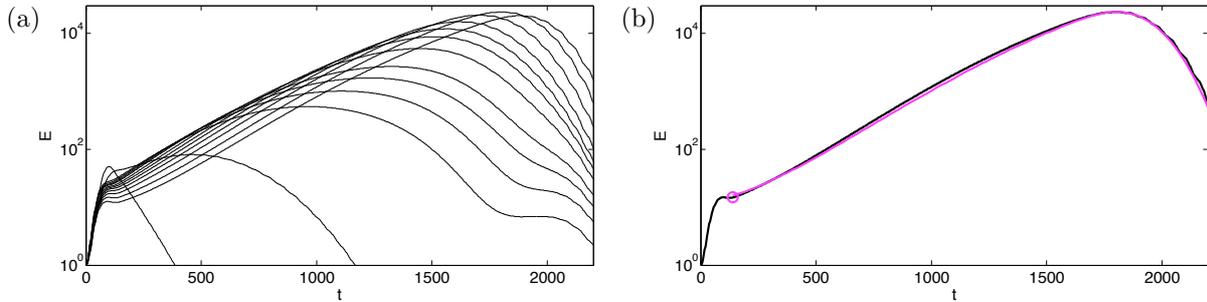
Figure 3. (a) Energy growth when optimizing for different times. The maximum is achieved for time $t = 1800$ for which the maximum energy is $E = 2.35 \cdot 10^4$. (b) Thin black line repeats the energy evolution leading to the maximum growth at $t = 1800$, whereas thick magenta line shows the energy evolution obtained when projecting the system onto a small number of eigenvectors related to the TS branch in Figure 2a. The latter clearly does not account for the initial gain due to the Orr mechanism, but by rescaling and shifting in time the two curves collapse, showing that the long time evolution is governed by propagating TS waves.

possible to project the system (7) on a set the set of eigenmodes obtained from (6), thereby approximating the optimal growth by a low-dimensional model of the flow.[1] For some flow configurations, where the degree of non-normality is rather small, only a few of the eigenmodes are needed to describe the dynamics of the flow. An example is the shallow rounded cavity flow in Ref. 26, where an oscillating cycle could be captured by the sum of two unstable eigenmodes, and the detailed evolution of the Kelvin–Helmholtz waves could be captured by $\mathcal{O}(100)$ eigenmodes. However for a similar boundary layer flow as studied here Ref. 25 showed that $\mathcal{O}(1000)$ eigenmodes are needed to capture the combined effect of the Orr mechanism and the TS wavepacket evolution. With the present discretization and boundary conditions, however, the sum of the 1500 eigenmodes obtained from the Arnoldi method is not able to correctly describe the Orr mechanism as obtained by the optimization via the time-stepper defined in (8). This points to the limitations of using eigenvalues in complex systems characterized by strong non-normality.

Figure 3a shows the energy evolution when solving for the largest eigenvalues of (8) at times $t = \{100, 200, \ldots, 2000\}$. When optimizing for short times the optimal initial condition consist of upstream tilted structures that exploit the Orr mechanism only.[25] As we go toward longer time optimization the tilted structures move upstream, towards the start of our computational domain, weighting the possibility of growth due to the Orr and the TS mechanism. We find that the maximum growth in this box is obtained

American Institute of Aeronautics and Astronautics
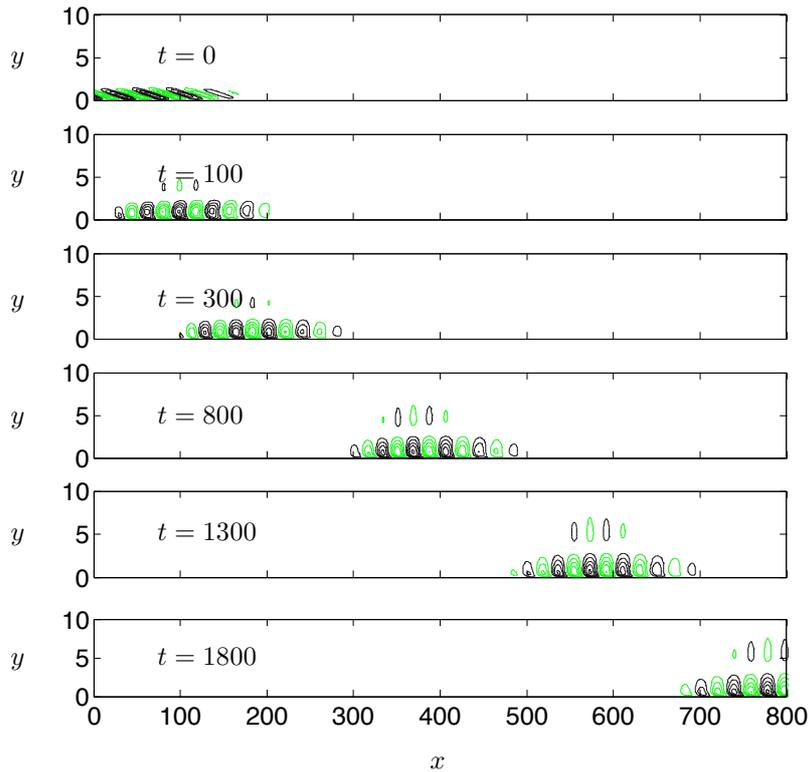
Figure 4. Time evolution for streamwise velocity with the combined Orr and TS mechanism, when initiated with the optimal initial condition from $t = 1800$. Note that the maximum amplitude is growing from frame to frame following the energy evolution given in Figure 3(b).

for the time $t = 1800$. The corresponding optimal initial condition is shown in the top frame in Figure 4. In figure 3b we compare the energy evolution due to that initial condition with the energy evolution obtained when projecting (8) onto a small number of modes related to the TS branch in Figure 2. The projected system clearly does not capture the initial energy gain due to the Orr mechanism, but by rescaling the energy curve and shifting it in time to account for the initial gain due to the Orr mechanism we see that the subsequent evolution is almost perfectly matching the full system. The detailed evolution of the streamwise velocity due to the optimal initial condition at time $t = 1800$ is shown in Figure 4. At the initial time the structures are leaning backwards against the shear. During the initial phase of the development the disturbance is raised up, exploiting the Orr mechanism, forming a wavepacket consisting of TS-waves. The wavepacket then propagates downstream, grows in size and finally leaves the computational domain, following the energy evolution in figure 3b.

IV.   Input-Output Analysis

As mentioned above, fluid flow systems are characterized by a large number of degrees of freedom. Therefore, to apply modern control theory to design efficient flow manipulation it is important to construct a reduced order model of the system. The main features of the flow behavior which is relevant to maintain in the reduced order model is the input-output behavior of the system, *i.e.* the relation between actuation and sensor output since the disturbances are represented by an input and the objective consists of minimizing an output signal. As a consequence, turning our attention to the particular solution with $q_0 = 0$, the input-output (I/O) relation can be written

$$y(t) = C \int_0^t e^{A(t-\tau)} B f(\tau) \, d\tau. \tag{9}$$

Rather than investigating flow fields at different times, the I/O behavior considers the time signals, $f(t)$ and $y(t)$. Fortunately, the I/O behavior has significantly simpler dynamics compared to stability analysis where

American Institute of Aeronautics and Astronautics
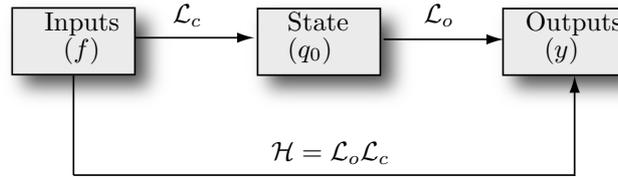
Figure 5. The operators used to examine the system input-output behavior. The controllability operator $\mathcal{L}_c$ relates past inputs to the present state, while the observability mapping $\mathcal{L}_o$ relates the present state to the future outputs. Their combined action is expressed by the Hankel operator $\mathcal{H}$.

the entire flow dynamics is under investigation.

The model reduction problem for the preservation of input-output dynamics can thus be posed as: Find the state-space system

$$\frac{\mathrm{d}\kappa}{\mathrm{d}t} = \hat{A}\kappa + \hat{B}f, \tag{10}$$

$$\hat{y} = \hat{C}\kappa. \tag{11}$$

so that for any input f, $\|y - \hat{y}\| \leq \epsilon$ where $\epsilon \ll 1$ and $\hat{y}$ the output of the model. The reduced-order system (11) can be obtained by a Galerkin projection onto a small number of modes, typically less than $m < 100$. The transfer function associated with stable state-space system is defined as the Laplace transform of (9)

$$y(s) = G(s)f(s) = C(sI - A)^{-1}Bf(s) \qquad s \in \mathcal{C}. \tag{12}$$

The model reduction error is commonly given by

$$\|G(s) - \hat{G}(s)\| \leq \epsilon, \tag{13}$$

with $\hat{G} = \hat{C}(sI - \hat{A})^{-1}\hat{B}$.

IV.A. Balanced modes

One way to compute the reduced-order model (11) with a nearly minimal model reduction error (13) is called balanced truncation.[6] We outline the method by defining the mapping from past inputs to future outputs via the Hankel operator,[27]

$$y(t) = \mathcal{H}f(t) = C\int_{-\infty}^{0} e^{A(t-\tau)}Bf(\tau)\,\mathrm{d}\tau. \tag{14}$$

The difference of the above expression and the formal solution (9) is that the Hankel operator (14) characterizes the I/O behavior via a reference state q_0. As shown schematically in Figure 5, the Hankel operator can be decomposed into

$$\mathcal{H} = \mathcal{L}_o \mathcal{L}_c \tag{15}$$

where the controllability operator $\mathcal{L}_c$ is defined as

$$q_0 = \mathcal{L}_c f(t) = \int_{-\infty}^{0} e^{-A\tau}Bf(\tau)\,\mathrm{d}\tau, \tag{16}$$

and the observability operator $\mathcal{L}_o$ is defined as

$$y(t) = \mathcal{L}_o(t)q_0 = Ce^{At}q_0. \tag{17}$$

The operator $\mathcal{L}_c$ describes the mapping of any input $f(t)$ with $t \in (-\infty, 0]$ onto the state vector q_0 at the reference time $t = 0$. The action of $\mathcal{L}_c$ can be numerically computed by a time-stepper. It amounts to solving the linearized Navier–Stokes equations for the velocity field q with forcing term $f(t)$ and zero initial conditions. The operator $\mathcal{L}_o$ describes the mapping of any initial velocity field q_0 to the output signal $y(t)$. The action of $\mathcal{L}_o(t)$ can also be numerically computed and it amounts to extracting the output signal while

American Institute of Aeronautics and Astronautics
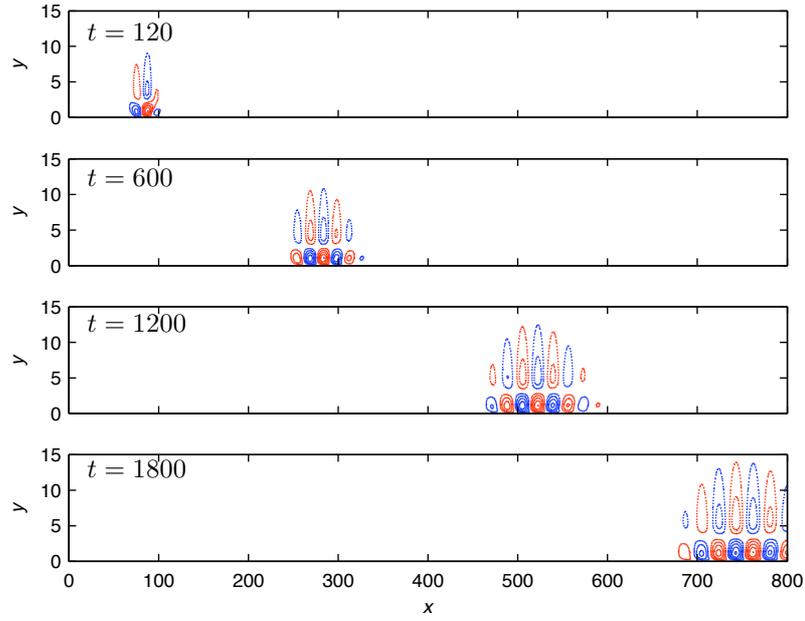
Figure 6. Instantaneous snapshots of the streamwise disturbance component at $t = 120, 600, 1200$ **and** 1800**.**

solving the linearized Navier–Stokes equations with the initial condition q_0 at the reference time $t = 0$ and zero forcing.

Similar to the short-time stability analysis using the expression (7) and (8), the I/O analysis can be reduced to an eigenvalue problem. The amplification of the output signal at time t is given by

$$\|y(t)\| = (\mathcal{H}(t)f, \mathcal{H}(t)f) = (f, \mathcal{H}^*(t)\mathcal{H}(t)f). \tag{18}$$

In particular, the eigenmodes f_j of $\mathcal{H}^*\mathcal{H}$ result in the largest output response, *i.e.*

$$\mathcal{H}^*\mathcal{H}f_j = \sigma_j^2 f_j \tag{19}$$

where σ_j are called the Hankel singular values and inputs f_j have unit norm. The model reduction error of balanced truncation is for a reduced-order model of order m is

$$\sigma_{m+1} < \|G(s) - \hat{G}(s)\|_\infty \leq 2 \sum_{j=m+1}^{n} \sigma_j. \tag{20}$$

Using the mapping $\mathcal{L}_c$ we can now obtain a set of function $\{\phi_j\}_{j=1}^m$ by mapping the eigenvectors of $\mathcal{H}^*\mathcal{H}$ onto state-space, *i.e.*

$$\phi_j = \mathcal{L}_c f_j. \tag{21}$$

The balanced modes are non-orthogonal, and set of modes that are bi-orthogonal to ϕ_j $((\phi_i, \psi_j) = \delta_{i,j})$ can be found from

$$\psi_j = \mathcal{L}_o^* g_j, \tag{22}$$

where g_j are the eigenvectors of $\mathcal{H}\mathcal{H}^*$ and $\mathcal{L}_o^* = \int_0^\infty e^{A^H t} C^H \, dt$ the adjoint of $\mathcal{L}_o$.

Traditionally, the balanced modes are defined as the eigenvectors of the product of the controllability and observability Gramian. This formulation is easily obtained by noting that

$$\mathcal{L}_c \mathcal{H}^*\mathcal{H}f_j = \underbrace{\mathcal{L}_c \mathcal{L}_c^*}_{P} \underbrace{\mathcal{L}_o^* \mathcal{L}_o}_{Q} \underbrace{\mathcal{L}_c f_j}_{\phi_j} = \sigma^2 \underbrace{\mathcal{L}_c f_j}_{\phi_j} \tag{23}$$

with the controllability Gramian

$$P = \mathcal{L}_c \mathcal{L}_c^* = \int_0^\infty e^{At} B B^H e^{A^H t} \, dt, \tag{24}$$

American Institute of Aeronautics and Astronautics
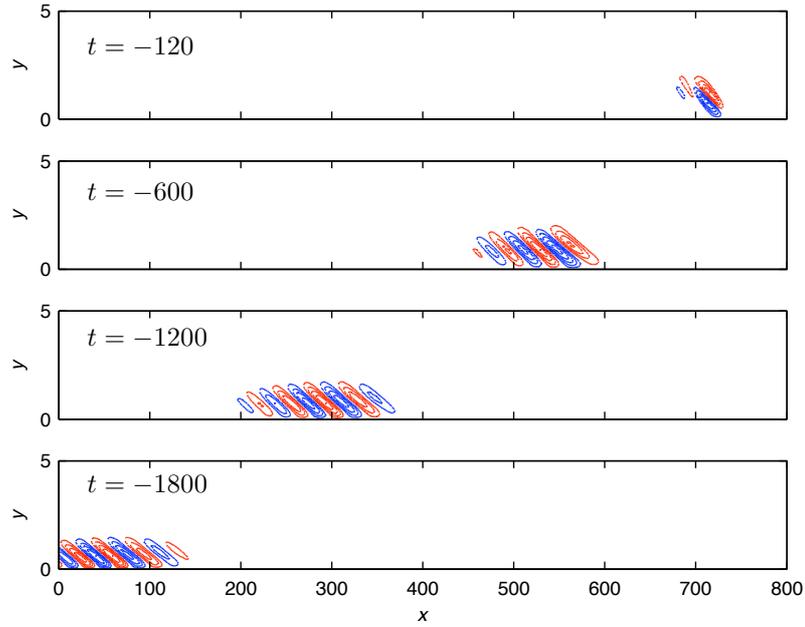
Figure 7. Instantaneous snapshots of the streamwise disturbance component at $t = -120, -600, -1200$ **and** -1800 **of the adjoint equations.**

and observability Gramian

$$Q = \mathcal{L}_o^* \mathcal{L}_o = \int_0^\infty e^{A^H t} C^H C e^{At} \, dt. \tag{25}$$

By recognizing that (24) and (25) are the state correlation matrices of the forward and adjoint state forced by impulses at the input and output respectively, the snapshot technique[28] can be employed to compute the balanced modes. The method is described in detail in Ref. 7: it amounts to collect a set of snapshots from a forward simulation using the input B as initial condition

$$X = [u(t_1), \dots, u(t_m)]\Delta, \tag{26}$$

and a set of snapshots from an adjoint simulation using the output C as initial condition,

$$Y = [p(t_1), \dots, p(t_m)]\Delta. \tag{27}$$

In the above, Δ contains the square root of the quadrature weights of the time-integrals given in (24) and (25). Snapshots of the forward and adjoint simulation are displayed in figures 6 and 7. The eigenvalue problem (23) can then be approximated as

$$PQ\phi_j \approx \underbrace{XX^H YY^H}_{n \times n} \phi_j = \sigma^2 \phi_j. \tag{28}$$

This eigenvalue problem is of size $n \times n$ and prohibitively expensive to solve for Navier-Stokes system. In the method of snapshots the balanced modes are expanded in snapshots, $\phi = Xa$, in order to obtain an eigenvalue problem of size $m \times m$,

$$X(\underbrace{X^H YY^H X}_{m \times m} a - \sigma^2 a) = 0. \tag{29}$$

The balanced modes and their associated adjoint modes computed in this manner are shown in figure 8 and 9, respectively.
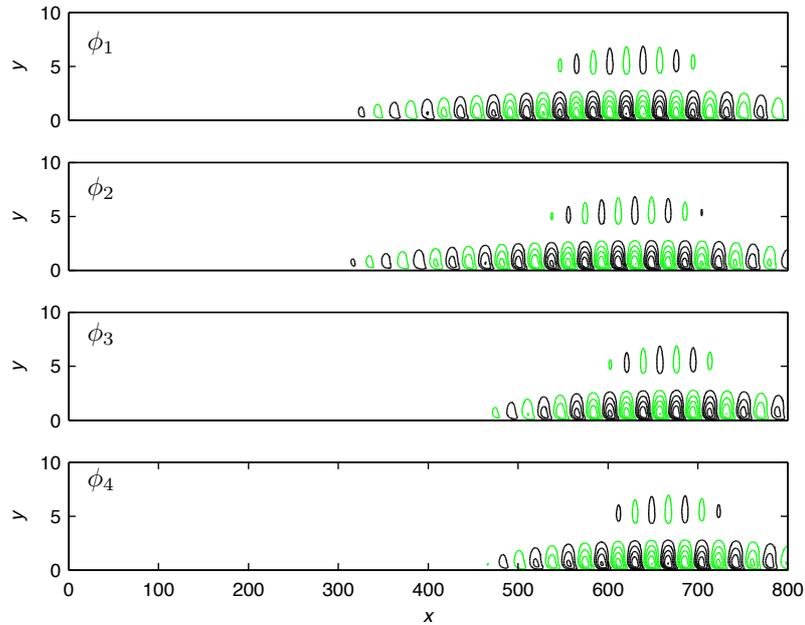
Figure 8. The streamwise velocity component of four first balanced modes ϕ_i.

IV.B. Model Reduction

To obtain the balanced reduced-order model (11) we can project Navier-Stokes equations including inputs and outputs on the balanced modes

$$A_{i,j} = (\psi_i, A\phi_j) \tag{30}$$

$$B_{1,j} = (\psi_j, B_1) \tag{31}$$

$$C_{1,j} = C_1\phi_j \tag{32}$$

and similarly for B_2 and C_2. The model reduction error is shown in figure 10 together with the theoretical bounds given by the Hankel singular values in (20)a. The infinity norm of the transfer function equals the peak value of the frequency response. Estimating the model reduction error amounts to the calculation of the difference of the peak values of the reduced-order and the Navier–Stokes system. The error norm remains within or lower than the bounds given by the HSV for the first 50 modes.

The amplitudes of the transfer functions with $s = i\omega$, *i.e.* the frequency response, are displayed in figure 10a for reduced-order models of order $r = 2, 50$ and 80 and for the full DNS model of order 10^5. From figure 10b we observe that the reduced-order model of order 2 captures the most important aspect of the input-output behavior, which is the response of the most dangerous frequency, *i.e.* the peak response of the full model. The model with 50 modes is able to estimate the gains of all the amplified frequencies, but fails to capture the damped low and high frequencies. Adding 30 additional modes results in a model that preserves the input-output behavior correctly for all frequencies.

Finally, the impulse response from all inputs to all outputs in the reduced-order model (11) and in the full Navier–Stokes system (2) is also compared. In figure (11) three signals $B_1 \to C_1$, $B_1 \to C_2$ and $B_2 \to C_1$ are shown with black lines. The response of C_2 to forcing in B_2 is zero, since disturbances traveling upstream are quickly damped. These impulse responses were obtained by using the time-stepper with $\sim 10^5$ degrees of freedom. The impulse responses of the reduced-order model (11) with $r = 50$ given by $y(t) = Ce^{At}B$ are shown with red dashed lines. We observe that reduced-model registers the same signal as the full model from all inputs to all outputs. The wavepacket triggered by the impulse of B_1 reaches the first sensor C_2 after 600 time units and the second sensor C_1 after 1500 time units. The wavepacket triggered from the actuator B_2 reaches the second sensor after 600 time units.

American Institute of Aeronautics and Astronautics
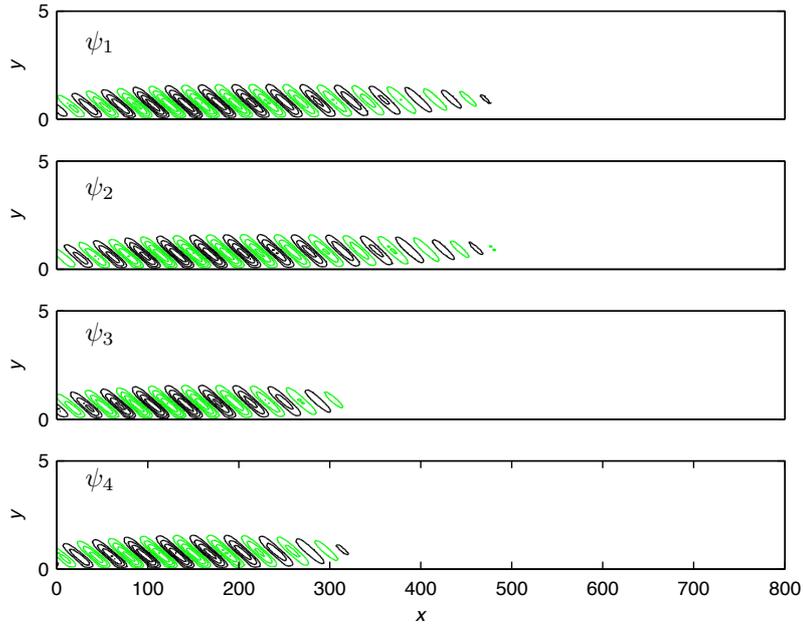
Figure 9. The streamwise velocity component of the adjoint balanced modes ψ_i.

V.   Control Design

The final step after the analysis of the response of a linear system to initial conditions and external excitations is to manipulate the inherent dynamics of a system or to control it. To this end, a reduced-order feedback controller, which will have the same dimension as the reduced-order model of the previous section, is developed. The closed-loop behavior of the system and the variations of the objective function will be investigated and compared to the uncontrolled case for the flat-plate boundary layer flow.

The reducer-order plant with three inputs $f = [f_1, g, f_2]^T$ and two outputs $y = [y_1, y_2]^T$ obtained from the model reduction procedure described in the previous section can be written,

$$\frac{\mathrm{d}\kappa}{\mathrm{d}t} = A\kappa + B_1 f_1 + B_2 f_2 \tag{33}$$

$$y_1 = C_1\kappa + lf_2, \tag{34}$$

$$y_2 = C_2\kappa + \alpha g. \tag{35}$$

Note again that the above state-system is the reduced-order model, the hats on A, B and C are dropped for convenience. The input f_1 represents disturbances whereas f_2 is the control signal (see Figure 1). Note that additional forcing terms appear also in the definition of the output signal. The first output y_1 can be regarded as the objective function,

$$\|y_1\|^2 = \|C_1\kappa\|^2 + l^2\|f_2\|^2 = \int_0^T \left(\kappa^H C_1^H C_1 \kappa + l^2 f_2^H f_2 \right) \mathrm{d}t, \tag{36}$$

where it is assumed that the cross weighting between the state and control signal is zero.[29] For large values of the scalar l the control effort is considered to be expensive, whereas small values indicate cheap control. The second output y_2 is forced with noise g to model the uncertainty that may exists in the measurements under realistic conditions. Large values of the scalar α indicate high level of noise corruption in the output signal, whereas for low values of α the measurement y_2 reflects information about the flow field with high fidelity.

For our purpouses the so called $\mathcal{H}_2$ control problem can be formulated as follows:

Find an optimal control signal $f_2(t)$ based on the measurements $y_2(t)$ such that the in the presence of external disturbances $f_1(t)$ and measurement noise $g(t)$ the output $y_1(t)$ is minimized.

American Institute of Aeronautics and Astronautics
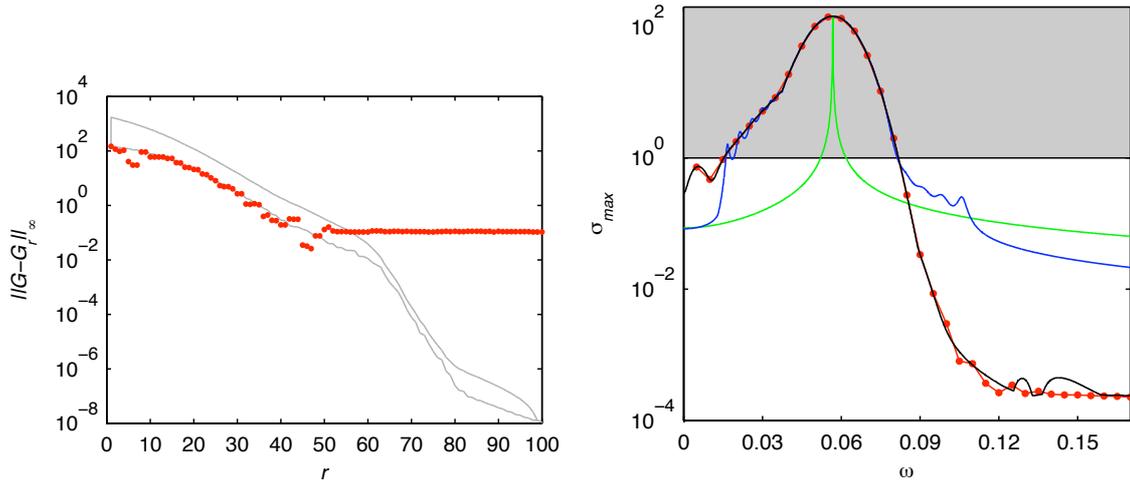
Figure 10. (a) The Hankel singular values σ_i corresponding to the balanced modes are shown with red symbols. The upper and lower theoretical bounds are depicted with gray lines. (b) The largest singular value of the transfer function $|G(i\omega)|$ from all input to all outputs computed using the time-stepper is shown with red symbols. The largest response is for $\omega = 0.06$ with a peak value of 144.6. The frequencies in the grey domain are amplified. The frequency response of the reduced model with rank 2 (green), 50 (blue) and 80 (black).

The solution to this control problem is obtained by solving two quadratic matrix Riccati equations.[29] These equations can be solved since the dimension of (33) is less than 100. The solution to the $\mathcal{H}_2$ control problem in a stochastic framework is also known as Linear Quadratic Gaussian, where stochastic processes are introduced to describe the sensor noise $g(t)$ and the external disturbances $f_1(t)$. We refer to Refs. 18, 30, 31 for further details on the $\mathcal{H}_2$ control algorithm, as we will only outline the main steps here.

The determination of the control signal is based only on the measurements from the sensor C_2. However, for linear systems — due to the separation principle[31] — the feedback control law can be determined assuming that the complete velocity field is known. The forcing needed to reproduce the flow only from wall measurements can be computed independently. Hence, the design of the $\mathcal{H}_2$-controller is performed in the following three steps:

(i) Compute the control feedback gain K by solving a Riccati equation to obtain the feedback type of control signal

$$f_1 = K\kappa. \tag{37}$$

This leads to a new system (compared to (11)),

$$\frac{\mathrm{d}\kappa}{\mathrm{d}t} = (A + B_2 K)\kappa + B_1 f_1, \tag{38}$$

$$y_1 = C_1 \kappa. \tag{39}$$

The resulting modified operator $A + B_2 K$ has dynamics that results in a smaller amplitude of the output signal y_1 than for the unperturbated operator A in (11).

(ii) Compute the estimation feedback gain L by solving a dual Riccati equation, to obtain the observer

$$\frac{\mathrm{d}\hat{\kappa}}{\mathrm{d}t} = (A + LC_2)\hat{\kappa} + Ly_2 \tag{40}$$

which is asymptotically stable, *i.e.* $\|\kappa - \hat{\kappa}\| \to 0$ as $t \to \infty$. This implies that the estimated state $\hat{\kappa}$ based on the measurements y_2 approaches the true state κ exponentially fast.

(iii) The closed-loop controller is finally obtained as

$$\frac{\mathrm{d}\hat{\kappa}}{\mathrm{d}t} = (A + B_2 K + LC_2)\hat{\kappa} - Ly_2, \tag{41}$$

$$f_2 = K\hat{\kappa}. \tag{42}$$

Given the measurements signal y_2 from the physical flow, the reduced-order controller provides an optimal control signal f_2 proportional to the estimated flow $\hat{\kappa}$.
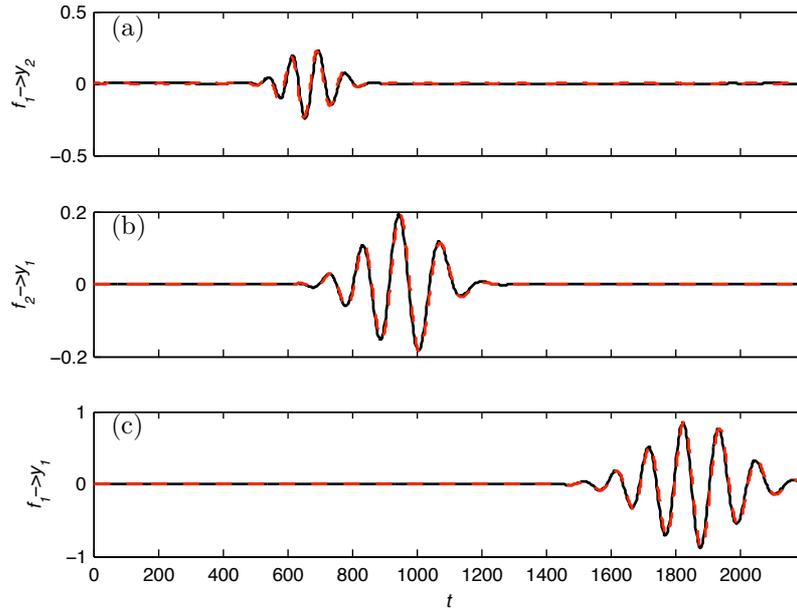
Figure 11. The impulse response from $B_1 \rightarrow C_2$ (a), $B_2 \rightarrow C_1$ (b) and $B_1 \rightarrow C_1$ (c). The black solid line represents direct numerical simulations with 10^5 degrees of freedom and the red dashed line the balanced reduced-model with 50 degrees of freedom.

We will now investigate the performance of the closed-loop system (42). In particular, the output y_1 of the closed-loop — with optimal control signal f_2 — and of the linearized Navier–Stokes equations without control are considered in the case of stochastic excitation from f_1.

Three controllers are investigated: (i) cheap control/low noise contamination with $l = 0.1$ and $\alpha = 0.1$, (ii) expensive control/high noise contamination with $l = 10$ and $\alpha = 10$ and (iii) an intermediate case with $l = 2$ and $\alpha = 0.1$.

Note that the purpose of the measurement noise g is to account for uncertainties in the sensor measurements during the control design. When evaluating the closed-loop performance — solving the controlled Navier–Stokes equations — the system is only forced with f_1 and not with g.

The performance of the control in case (i) is examined first. In figure 12 the input and output signals are shown. The gray region indicates the time when the control is active. As disturbance signal $f_1(t)$ we choose white noise; the corresponding response of the sensor $y_2(t)$ in figure 12b confirms the amplification and filtering of the signal as it traverses the unstable domain. The disturbances reach the second sensor (figure 12d) after about 1500 time units where they have been amplified by one order of magnitude. The control is activated at time $t = 2500$, the actuator immediately begins to force the system with a control signal (figure 12c) based on the output y_1, and after a delay of another 1500 time units, the stabilizing effect of the control signal on the output f_1 is clear. When the control is deactivated (at $t = 7500$) the disturbances start to grow again.

The wall-normal maximum of the rms-values of the streamwise velocity component in cases with and without control are shown in figure 13. The rms-value grows exponentially downstream in the uncontrolled case until the fringe region at $x = 800$. The rms of the controlled perturbation grows only until it reaches the actuator position where it immediately begins to decay. At the location of the objective function C_1 ($x = 750$), the amplitude of the perturbations is one order of magnitude smaller than in the uncontrolled case for the cheapest controller.

The rms values in the case of the expensive (case ii) and intermediate control (case iii) are shown with dashed and dashed-dotted lines respectively. The expensive control is very conservative as the measurement signals are highly corrupted and the control effort limited; it results only in a small damping of the disturbances. The intermediate controller (case iii) is more cautious in reducing the perturbation energy just downstream of the actuator when compared to the cheap controller. It is interesting to note, however, that at the location where the objective function is measured, the disturbance amplitude has decreased nearly

American Institute of Aeronautics and Astronautics
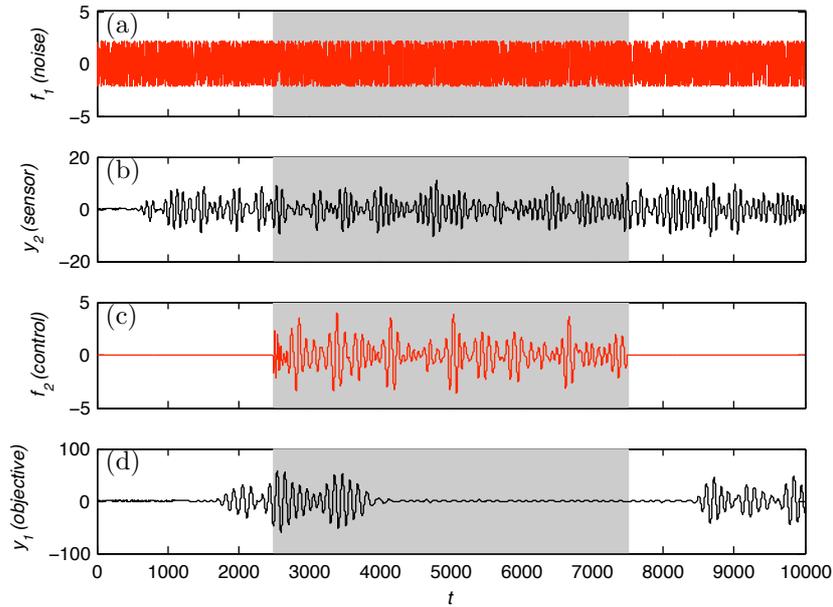
Figure 12. Input and output signals of the closed-loop system. The the random forcing f_1 (a), measurements signal y_2 (b), control signal f_2 (c) and the objective function y_1 (d) is shown. The cheap controller is active between $t \in [2500, 7500]$ marked with the gray area.
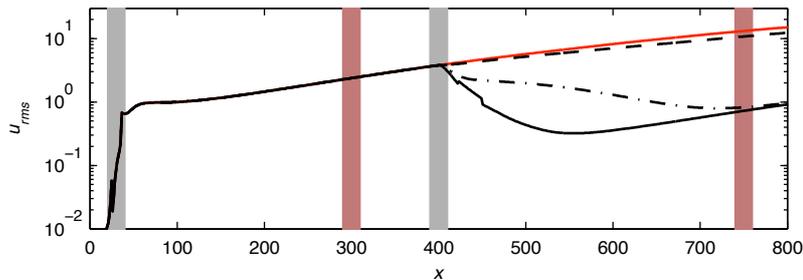
Figure 13. The rms-values of the uncontrolled system (red line), cheap controller (solid black), intermediate controller (dashed-dotted line) and expensive controller (dashed line). The gray bar represent the size (defined as 99% of the spatial support) and location of the two inputs, whereas the red bars correspond to the two outputs.

as much as with the cheap controller, although the total perturbation energy is much larger over the entire domain.

VI.   Conclusion

A unified framework for the stability and input-output analysis, model reduction and control design of complex flows is presented. The two-dimensional Blasius boundary-layer flow is used here as example of a spatially inhomogeneous flow characterized by strong non-normality of the operator describing the linear evolution of velocity perturbations.[3] The approach followed here requires only the numerical solution of the Navier–Stokes equations and of the associated dual problem, the so-called time-stepper approach.[5] It avoids therefore the manipulation of large matrices and can be extended to fully three-dimensional flows, complex geometries and physics.

It is shown how the stability of complex flows can be investigated by considering the eigenvalues of the governing linear operator computed through subspace iterative methods. However, the boundary layer flow considered here is characterized by convective instabilities and is therefore stable in a global sense. The amplification of unstable waves traveling downstream and leaving the control domain can be seen in this context as transient growth. Non-modal input-output analysis becomes therefore the correct tool to

analyze these flows.[3,4] Optimal initial conditions yielding the largest possible energy growth over a finite time horizon are obtained for the Blasius boundary layer by integrating the Navier-Stokes direct and adjoint equations in time. The results reproduce and extend those previously obtained by expanding the flow into the eigenmodes of the system.[25] In the case of strong non-normality a large number of eigenvectors of the system are needed and the time-stepper approach may become more efficient already for two-dimensional flows.

To apply tools from modern control theory to fluid flow systems with many degrees of freedom model reduction becomes unavoidable. To build a low-order model of the problem the main features of the flow behavior are investigated in an input-output framework. The quantity one wishes to optimize for is now defined by a sensor output, in our case the level of perturbations further downstream, while information to the controller is provided by a sensor located upstream. Perturbations are introduced by the inputs considered in the model: the input furthest upstream models incoming disturbances while a second actuator is used to manipulate the flow. The observable, controllable and balanced modes of the system can be computed by numerical simulations of the flow impulse response: controllable modes are approximated by the POD mode of the flow response to inputs, while observable structures can be computed as POD modes of the response of the adjoint system to excitations from the outputs. Balanced modes are computed also from snapshots of the flow as introduced in Ref. 7. The analysis can be seen as an extension of the stability analysis mentioned above,where inputs and outputs are taken into account.

Model reduction is achieved by projecting the governing equations on the leading balanced modes of the system. We show that the input-output behavior of the flat-plate boundary layer can be captured accurately with a reduced-order model based on fifty balanced modes. These modes are shown to provide a good description of the flow[9,18] since the account for both observability and controllability through a non-orthogonal projection. The spatial structure of these modes reflect the location of sensors/actuators and the dynamics of linear perturbation evolving in a boundary layer. The balances modes are mainly located downstream, where the response to the forcing is largest. The adjoint balanced modes are instead located upstream, where the sensitivity to initial conditions is the largest.

Finally, the low-order model is used to obtain the feedback gain relating directly the measurements from one upstream sensor to the actuator signal using the $\mathcal{H}_2$ formulation. The control is then applied in the numerical simulation of the full system where we show that the perturbations growth could be reduced efficiently. The present formulation accounts naturally for localized sensors and actuators and therefore, it can be directly applied to different flow configurations. Further, the control law derived from the low-order system can be applied on-line in an experiment provided accurate modeling of the sensor and actuator is available for the I/O analysis.

Acknowledgments

References

[1]Schmid, P. J. and Henningson, D. S., *Stability and transition in shear flows*, Springer, 2001.

[2]Huerre, P. and Monkewitz, P. A., "Local and Global Instabilities in Spatially Developing Flows," *Annu. Rev. Fluid Mech.*, Vol. 22, 1990, pp. 473–537.

[3]Chomaz, J. M., "Global Instabilities in Spatially Developing Flows: Non-normality and Nonlinearity," *Ann. Rev. Fluid Mech.*, Vol. 37, 2005, pp. 357–392.

[4]Schmid, P. J., "Nonmodal Stability Theory," *Ann. Rev. Fluid Mech.*, Vol. 39, 2007, pp. 129–62.

[5]Barkley, D., Gomes, M. G., and Henderson, R. D., "Three-dimensional Instability in Flow Over a Backward-facing Step," *J. Fluid Mech.*, Vol. 473, 2002, pp. 167–190.

[6]Moore, B., "Principal component analysis in linear systems: Controllability, observability, and model reduction," *Automatic Control, IEEE Transactions*, Vol. 26, No. 1, 1981, pp. 17–32.

[7]Rowley, C. W., "Model Reduction for Fluids Using Balanced Proper Orthogonal Decomposition," *Int. J. Bifurc. Chaos*, Vol. 15, No. 3, 2005, pp. 997–1013.

[8]Willcox, K. and Peraire, J., "Balanced Model Reduction Via the Proper Orthogonal Decomposition," *AIAA J.*, Vol. 40, No. 11, 2002, pp. 2323–2330.

[9] Ilak, M. and Rowley, C. W., "Modeling of Transitional Channel Flow Using Balanced Proper Orthogonal Decomposition," *Phys. Fluids*, Vol. 20, 2008, pp. 034103.

[10] Ahuja, S., Rowley, C. W., Kevrekidis, I. G., and Wei, M., "Low-dimensional Models for Control of Leading-edge Vortices: Equilibria and Linearized Models," *AIAA Paper 2007-709, 45th AIAA Aerospace Sciences Meeting and Exhibit*, 2007.

[11] Kim, J. and Bewley, T. R., "A Linear Systems Approach to Flow Control," *Annu. Rev. Fluid Mech.*, Vol. 39, 2007, pp. 383–417.

[12] Högberg, M. and Henningson, D. S., "Linear optimal control applied to instabilities in spatially developing boundary layers," *J. Fluid Mech.*, Vol. 470, 2002, pp. 151–179.

[13] Högberg, M., Bewley, T. R., and Henningson, D. S., "Relaminarization of $Re_\tau = 100$ turbulence using gain scheduling and linear state-feedback control." *Phys. Fluids*, Vol. 15, 2003, pp. 3572–3575.

[14] Hoepffner, J., Chevalier, M., Bewley, T. R., and Henningson, D. S., "State estimation in wall-bounded flow systems. Part 1. Perturbed laminar flows," *J. Fluid Mech.*, Vol. 534, 2005, pp. 263–294.

[15] Chevalier, M., Hoepffner, J., Bewley, T. R., and Henningson, D. S., "State estimation in wall-bounded flow systems. Part 2. Turbulent flows," *J. Fluid Mech.*, Vol. 552, 2006, 167-187.

[16] Chevalier, M., Hoepffner, J., Åkervik, E., and Henningson, D. S., "Linear feedback control and estimation applied to instabilities in spatially developing boundary layers." *J. Fluid Mech.*, Vol. 588, 2007, pp. 163–187.

[17] Monokrousos, A., Brandt, L., Schlatter, P., and Henningson, D. S., "DNS and LES of estimation and control of transition in boundary layers subject to free-stream turbulence," *Int. J. Heat Fluid Flow*, Vol. 29, No. 3, 2008, pp. 841–855.

[18] Bagheri, S., Hœpffner, J., Schmid, P., and Henningson, D., "Input-Output Analysis and Control Design Applied to a Linear Model of Spatially Developing Flows," *Appl. Mech. Rev.*, 2008, In press.

[19] White, F. M., *Viscous Fluid Flow*, McGraw–Hill, Inc, second edition ed., 1991.

[20] Chevalier, M., Schlatter, P., Lundbladh, A., and D.S., H., "A pseudo spectral solver for incompressible boundary layer flows," *Technical Report, Trita-Mek*, Vol. 7, 2007.

[21] Molder, C. and Van Loan, C., "Ninteen dubios ways to compute the exponential of a matrix, twenty-five years later," *Siam Review*, Vol. 45, 2003, pp. 3–000.

[22] Giles, M. B. and Pierce, N. A., "An introduction to the adjoint approach design," *Flow, Turbulence and Combustion*, Vol. 65, No. 3/4, 2000, pp. 393–415.

[23] Bagheri, S., Brandt, L., and Henningson, D. S., "Input-output analysis, model reduction and control design of the flat-plate boundary layer," *J. Fluid Mech.*, 2008, Submitted.

[24] Lehoucq, R. B., Sorensen, D., and Yang, C., *ARPACK Users' Guide: Solution of Large-Scale Eigenvalue Problems with Implicitly Restarted Arnoldi Methods*, SIAM, Philadelphia, 1998.

[25] Åkervik, E., Ehrenstein, U., Gallaire, F., and Henningson, D. S., "Global two-dimensional stability measures of the flat plate boundary-layer flow," *Eur. J. Mech. B/Fluids*, 2007, In press.

[26] Åkervik, E., Hœpffner, J., Ehrenstein, U., and Henningson, D. S., "Optimal Growth, Model Reduction and Control in a Separated Boundary-layer Flow Using Global Eigenmodes," *J. Fluid. Mech.*, Vol. 579, 2007, pp. 305–314.

[27] Glover, K., "All optimal Hankel-norm approximations of linear multivariable systems and the L^∞-error bounds," *Int. J. Control*, Vol. 39, 1999, pp. 1115–1193.

[28] Sirovich, L., "Turbulence and the Dynamics of Coherent Structures I-III," *Quart. Appl. Math.*, Vol. 45, 1987, pp. 561–590.

[29] Zhou, K., Salomon, G., and Wu, E., "Balanced Realization and Model Reduction for Unstable Systems," *Int. J. Robust Nonlinear Control*, Vol. 9, 1999, pp. 183–198.

[30] Anderson, B. and Moore, J., *Optimal control: Linear Quadratic Methods*, Prentice Hall, New York, 1990.

[31] Zhou, K., Doyle, J., and Glover, K., *Robust and Optimal Control*, Prentice Hall, New Jersey, 2002.